

Detectability of a phase transition in neutron star matter with third-generation gravitational wave interferometers

C. Mondal,^{1,2,*} M. Antonelli,^{1,†} F. Gulminelli,^{1,‡} M. Mancini,^{3,4,§} J. Novak,^{4,¶} and M. Oertel^{4,**}

¹*Normandie Univ., ENSICAEN, UNICAEN, CNRS/IN2P3, LPC Caen, 14000 Caen, France*

²*Institut d'Astronomie et d'Astrophysique, Université Libre de Bruxelles, CP 226, B-1050 Brussels, Belgium*

³*IDP, UMR 7013 - CNRS - Univ. Orléans- Univ. Tours. Université d'Orléans,*

rue de Chartres, BP 6759, 45067 Orléans Cedex 2, France

⁴*Laboratoire Univers et Théories, Observatoire de Paris, Université PSL, CNRS, 92190 Meudon, France*

Possible strong first-order hadron-quark phase transitions in neutron star interiors leave an imprint on gravitational waves, which could be detected with planned third-generation interferometers. Given a signal from the late inspiral of a binary neutron star (BNS) coalescence, assessing the presence of such a phase transition depends on the precision that can be attained in the determination of the tidal deformability parameter, as well as on the model used to describe the hybrid star equation of state. For the latter, we employ here a phenomenological meta-modelling of the equation of state that largely spans the parameter space associated with both the low density phase and the quark high density compatible with current constraints. We show that with a network of third-generation detectors, a single loud BNS event might be sufficient to infer the presence of a phase transition at low baryon densities with an average Bayes factor $B \approx 100$, up to a luminosity distance ($\mathcal{D}_L \lesssim 300$ Mpc).

I. INTRODUCTION

In the standard picture, the interior of a neutron star (NS) encompasses several phases of matter, from nuclei in the iron region close to the surface via more exotic neutron-rich nuclear clusters in the crust to a uniform liquid of nuclear matter in the outer core [1]. In the core, at densities above nuclear saturation, $n_0 \approx 0.16 \text{ fm}^{-3}$, the pressure becomes so high that further degrees of freedom may emerge. These include, possibly, mesons –which could also form condensates–, hyperons or Δ -baryons. An even more dramatic possibility is that of a phase transition to degenerate quark matter and the formation of so-called hybrid stars. Under the hypothesis of absolutely stable strange quark matter, even pure quark stars might exist, see e.g. the reviews [2–6]. This makes the compact objects a unique testbed of subatomic physics, not only probing nuclear many-body phenomena and their dependence on density and isospin asymmetry, i.e. the neutron-to-proton ratio but also probing unexplored finite-density regimes of quantum chromodynamics.

Currently, the main astrophysical constraints on NS interiors stem from the precise mass determinations for three NSs in NS-white dwarf systems [7–10], all three with gravitational masses around $2 M_\odot$. The object PSR J0740+6620 [10] is thereby particularly interesting since NICER succeeded in obtaining a measurement of its radius [11, 12], making it the second object after

PSR J0030+0451 [13, 14] for which both mass and radius could be determined. Moreover, with the detections of gravitational waves from binary neutron star (BNS) mergers by the LIGO-Virgo collaboration, a new window has opened to explore the constituents of matter under extreme conditions. For the first detected event, GW170817, the tidal deformability was obtained [15], a quantity strongly correlated with the NS radius. In the coming years, starting with run O4 of the LIGO-Virgo-Kagra (LVK) collaboration, the gravitational wave (GW) detector network sensitivity will be further increased and a number of additional detections is expected. Projects for ground based third-generation detectors such as the European Einstein Telescope [16, 17] and the American Cosmic Explorer [18, 19] planned for ~ 2035 will allow for a considerable gain in sensitivity. They need more stringent constraints on theoretical models for the description of the dense matter.

A particular question in this context is the possible presence of a first-order phase transition (PT) in dense neutron star matter. Since the first mention of possible hybrid stars decades ago, e.g. [20], finding astrophysical signatures of such a PT has been a very active field of research, see for instance the reviews [21–23]. In this work, we investigate if and how accurately we can detect a PT in the core of two coalescing neutron stars during the inspiral phase with a network of third-generation gravitational wave detectors. Several authors have already pointed out that a PT in the post-merger phase leads to a characteristic increase in the dominant post-merger oscillation frequency [24, 25] with respect to the one expected from the measured inspiral parameters under the assumption of a purely baryonic equation of state (EoS). If the post-merger signal is detected it could even help to constrain the onset density for the phase transition [26] and a delayed PT could leave an imprint on the ringdown of the black hole formed once the metastable remnant has

* chiranjib.mondal@ulb.be

† antonelli@lpccaen.in2p3.fr

‡ gulminelli@lpccaen.in2p3.fr

§ marco.mancini@univ-orleans.fr

¶ jerome.novak@obspm.fr

** micaela.oertel@obspm.fr

collapsed [27]. These ideas apply if, prior to merger, both stars do not present any PT, which is plausible for not too massive stars.

The horizon for detecting a post-merger signal is, however, relatively small even for third-generation detectors and only a few events are expected, see e.g. [28]. On the contrary, a huge number of BNS mergers should be detected with information extracted from the inspiral among others about the chirp mass \mathcal{M}_c , the mass ratio q and on the combined tidal deformability $\tilde{\Lambda}$ (see Eq. (15)), which is a function of the tidal deformabilities Λ_1 and Λ_2 of both stars [17, 19, 29]. Since a PT changes the relation between the mass and the tidal deformability for each star, see e.g. [30–33], $\tilde{\Lambda}$ is modified, and this of course raises the question of its detectability which many studies have addressed recently.

For instance, based on the breakdown of quasi-universal relations fitted to purely hadronic EoS in [34] and a comparison of the inferred radius in [35] together with a collection of simulated BNS merger events for purely hadronic and hybrid EoS, it has been shown that ~ 50 -100 detections can be sufficient to distinguish different EoSs. In [36], the authors assess the possibility to distinguish different equation of state models with and without a PT from a GW170817-like event during the O4 run of LVK.

The above studies, however, conclude on the detectability of a PT by comparing a few EoS models, which is clearly not sufficient to cover the entire space of all possible EoSs with and without PT. A different approach has been used in [37, 38], where a non-parametric EoS inference is applied to the GW170817 event with weak statistical evidence in favor of two stable branches, i.e. the existence of hybrid stars with a strong PT. In the study by [39], the authors have performed a Bayesian inference study with three different injected EoS models, concluding that already 12 events with current detectors could be sufficient to disentangle a strong PT. However, the injected models represent only snapshots of all possible EoSs with a PT transition and the inference of a PT is done based on the number of different polytropes employed in the EoS reconstruction. Here, we will use a meta-modelling approach as well for the models with PT as for those without. The latter is a flexible parameterisation of the purely nuclear EoS, incorporating constraints from nuclear experiments, theory and astrophysical observations as priors [40]. For the former, we have extended the nuclear meta-model to include a potential PT taking as parameters the density for the onset of the transition, the energy density jump and the sound speed in the high-density phase controlling the stiffness of the EoS. The injection models have been chosen from the borders of the respective meta models. In addition, we will concentrate here on the possibility to detect a PT from one single loud event in third-generation detectors.

The paper is organised as follows: In section II we summarise the EoS modelling which is used in the present work. A brief summary of the Fisher matrix formalism

to quantify variances in various astrophysical parameters connected to a binary neutron star (BNS) merger is provided in section III. Section IV contains the proposed Bayesian framework to infer the possible signs of a PT from the gravitational wave signal generated by a BNS coalescence. We discuss the results in section V. Concluding remarks and the future extensions of the present work are discussed in section VI.

II. METAMODELLING OF NEUTRON STAR MATTER

For our purposes, NS matter comprises an inhomogeneous crust and a core of uniform matter fully governed by strong interaction. The crust and the purely nucleonic outer core are consistently calculated using the same energy functional, see section II B. We describe then the core, see section II A in the nucleonic hypothesis up to a certain density, beyond which we assume the appearance of quarks at the very center of the star. The density of the phase transition to the quark core is an input parameter in our model.

A. Neutron star core

1. Nucleonic part

For the description of the purely nucleonic outer core, we follow a metamodelling approach. Below we will briefly recall the main lines of the model, for details see [40]. Within our model, the uniform nucleonic matter is described by decomposing the energy density of infinite nuclear matter as

$$\varepsilon_N(n_n, n_p) = C_{kin} \sum_{q=n,p} \frac{n_q^{5/3}}{m_q^*(n, \delta)} + U_0(n) + U_{sym}(n) \delta^2 \quad (1)$$

where n_n (n_p) is the neutron (proton) number density, $n = n_n + n_p$ is the baryon number density, $\delta = (n_n - n_p)/n$ is the isospin asymmetry and $C_{kin} = 3(3\pi^2\hbar^3)^{2/3}/10 \approx 2.87\hbar^2$. The first term takes into account the zero point Fermi gas contribution, and the momentum dependence of the nuclear interaction through the density-dependent effective mass m_q^* ($q = n, p$). The remaining term is broken down into an isospin symmetric part, $U_0(n)$, and an isospin asymmetric part, $\delta^2 U_{sym}(n)$. For both $U_0(n)$ and $U_{sym}(n)$ an expansion up to order $N = 4$ around the nuclear saturation density n_{sat} is used:

$$U_{0,sym}(n) = n \sum_{k=0}^N \frac{(v_k)_{0,sym}}{k!} u_k^N(x) x^k, \quad (2)$$

with

$$x = \frac{n - n_{sat}}{3n_{sat}}, \quad \text{and,} \quad u_k^N(x) = 1 - (-3x)^{N+1-k} e^{-b(1+3x)}, \quad (3)$$

where the u_k^N terms ensure vanishing energy at zero density. The coefficients $(v_k)_{0, \text{sym}}$ are functions of nuclear matter properties (NMPs) at saturation density n_{sat} . Specifically, the coefficients of U_0 in Eq. (2) can be expressed as a function of the density derivatives at different orders of the energy per baryon of symmetric nuclear matter[41] (SNM), like the energy per particle E_{sat} , incompressibility K_{sat} , skewness Q_{sat} and kurtosis Z_{sat} . Similarly, the coefficients of U_{sym} are related to other NMPs, like the symmetry energy E_{sym} , symmetry slope L_{sym} , symmetry incompressibility K_{sym} , symmetry skewness Q_{sym} and symmetry kurtosis Z_{sym} , all evaluated at n_{sat} and for symmetric matter.

The contribution of an ideal gas of electrons (e) and muons (μ) to the energy density

$$\varepsilon_{e,\mu} = \frac{(m_{e,\mu})^4}{8\pi^2(\hbar c)^3} [(2x_r^2 + 1)x_r\gamma_r - \ln(x_r + \gamma_r)], \quad (4)$$

where, $x_r = \frac{\hbar c(3\pi^2 n_l)^{1/3}}{m_l}$ and $\gamma_r = \sqrt{1 + x_r^2}$ with $l = e, \mu$. The net amount of electrons present in the system is determined by the β -equilibrium condition solving the coupled equations of chemical potentials $\mu_{n,p,e}$ of neutrons, protons and electrons, respectively, as

$$\mu_n(n, \delta) - \mu_p(n, \delta) = \mu_e(n, \delta), \quad (5)$$

where $\mu_{n,p} = \partial \varepsilon_N / \partial n_{n,p} + m_{n,p} c^2$, and $m_{n,p}$ are the bare neutron and proton masses. If the chemical potential of electrons $\mu_e = \partial \varepsilon_e / \partial n_e$ exceeds the muon mass m_μ , they appear spontaneously in neutron star matter. Their amount is fixed by local charge equilibrium $n_\mu = n_p - n_e$, and the global equilibrium condition $\mu_\mu = \mu_e$. Once the equilibrium composition $\delta(n)$ is determined at each density from Eq. (5), the baryonic pressure is obtained from the thermodynamic relation

$$p_N(n) = \sum_{q=n,p} n_q (\mu_q - m_q c^2) - \varepsilon_N(n, \delta). \quad (6)$$

where n_q , μ_q and δ are all functions of n , while m_q are the two bare masses of neutrons and protons.

2. Quark matter EoS

We assume that the appearance of quarks in the inner core gives rise to a first-order phase transition, namely two continuous branches $p_N(\varepsilon_N)$, $p_Q(\varepsilon_Q)$ separated by a finite jump $\Delta\varepsilon$ in energy density at a given value p_t of the baryonic pressure. We note that ε_t is the highest value of the energy density in the nucleonic (N) phase, and $\varepsilon_t + \Delta\varepsilon$ represents the lowest energy density value in the quark phase. As a consequence, a discontinuity in the sound speed c_s between the nucleonic and quark phases is also expected. When the core gets converted to quarks completely, we assume it fixes c_s all the way up to the center of the neutron star from the point of

transition. In this simple picture, the EoS of the quark core can be specified by (see e.g. [42, 43]):

$$p_Q(\varepsilon_Q) = c_s^2(\varepsilon_Q - \varepsilon_t), \quad (7)$$

$$\mu_Q(p_Q) = \mu_t \left[1 + \frac{1 + c_s^2 p_Q}{c_s^2 \varepsilon_t} \right]^{c_s^2/(1+c_s^2)}, \quad (8)$$

$$n_Q(p_Q) = n_t \left[1 + \frac{1 + c_s^2 p_Q}{c_s^2 \varepsilon_t} \right]^{1/(1+c_s^2)} = n_t \left(\frac{\mu_Q}{\mu_t} \right)^{1/c_s^2} \quad (9)$$

Here, μ_t represents the baryonic chemical potential at the transition point ($\mu_B = \mu_n$ in the nucleonic phase), and n_t is the baryonic density at the onset of the transition. Three parameters n_t , c_s^2 and $\Delta\varepsilon$ are used on top of the parameters for the nucleonic metamodelling to describe the neutron star core. In [44] a similar approach is used to model the neutron star EoS in order to obtain constraints on a potential hadron-quark transition from neutron star observables, but the nucleonic part in their case is limited to one single EoS, obtained by fixing the NMPs to a fiducial set.

B. Neutron star Crust

We model the neutron star crust by using the compressible liquid drop model (CLDM) approximation of [45], which allows us to extend the metamodel for uniform nucleonic matter in Sec. II A 1. In the CLDM, the bulk energy of a spherical nucleus with A nucleons, Z protons, radius r_N and bulk density n_i is described by using Eq. (1) as $E_{\text{bulk}} = A\varepsilon_N(n_i, 1 - 2Z/A)/n_i$. The total binding energy of a finite nucleus is obtained by adding surface, curvature and Coulomb terms. The surface and curvature contributions are expressed in terms of surface and curvature tensions σ_s and σ_c as [46–48]

$$E_{\text{surf}} + E_{\text{curv}} = 4\pi r_N^2 \left(\sigma_s(Z/A) + \frac{2\sigma_c(Z/A)}{r_N} \right) \quad (10)$$

$$\text{with,} \quad \sigma_s(x) = \sigma_0 \frac{2^4 + b_s}{x^{-3} + b_s + (1-x)^{-3}}, \quad (11)$$

$$\sigma_c(x) = 5.5\sigma_s(x) \frac{\sigma_{0,c}}{\sigma_0} (\beta - x). \quad (12)$$

Finally, the Coulomb term in a spherical Wigner-Seitz (WS) cell reads:

$$E_{\text{coul}} = \frac{8}{3} \left(\pi e \frac{Z}{A} n_i \right)^2 r_N^5 \eta_{\text{coul}} \left(\frac{r_N}{r_{\text{WS}}} \right), \quad (13)$$

$$\text{with} \quad \eta_{\text{coul}}(x) = \frac{1}{5} \left[x^3 + 2 \left(1 - \frac{3}{2}x \right) \right]. \quad (14)$$

Here, e is the elementary charge, r_{WS} the radius of a WS cell, and η_{coul} the function taking into account electron screening in the Coulomb energy. The parameters σ_0 , $\sigma_{0,c}$, b_s and β are obtained by optimizing the agreement of nuclear masses in vacuum with the AME2016 mass table [49–51]. The EoS is eventually obtained

by minimizing the energy of the WS cell by varying A, Z, n_i, r_N, r_{WS} , as well as the neutron gas density n_g [45, 50, 51].

III. ESTIMATION OF DETECTORS' RESPONSE: FISHER INFORMATION FORMALISM

In order to assess the uncertainty in the parameter estimation associated with future observations of GWs from the coalescence of BNSs, we make use of the publicly available tool `GWBENCH` [52], which implements the Fisher information paradigm [53, 54]. The main drawback of this approach is that it is valid for events with a high signal-to-noise ratio (SNR) [55]. On the other hand, its main advantage is the considerable increase in computational speed, as compared to standard Bayesian analysis. Here we give a summary of our procedure to compute a sequence of simulated GW events from BNSs and estimate the parameters that could be inferred from such events by the third-generation Earth-based GW detectors. For details about `GWBENCH`, the interested reader can refer to [52].

We model events of BNS coalescence with masses m_1 and m_2 by using the waveform templates implemented in `GWBENCH`, namely the ‘‘TaylorF2 + tidal’’ models [56]. They depend on the following parameters: $(\mathcal{M}_c, \eta, \vec{\chi}_1, \vec{\chi}_2, \mathcal{D}_L, \iota, \tilde{\Lambda}, \delta\tilde{\Lambda})$. Here, $\eta = m_1 m_2 / (m_1 + m_2)^2$, $\vec{\chi}_{1,2}$ are the dimensionless spin vectors of the two NSs, \mathcal{D}_L is the luminosity distance, ι is the inclination angle of its orbital plane with respect to the line of sight. Finally, $\tilde{\Lambda}$ and $\delta\tilde{\Lambda}$ are two parameters containing the tidal deformabilities of both stars (Λ_1, Λ_2) and are defined as:

$$\tilde{\Lambda} = \frac{8}{13} [(1 + 7\eta - 31\eta^2) (\Lambda_1 + \Lambda_2) + \sqrt{1 - 4\eta} (1 + 9\eta - 11\eta^2) (\Lambda_1 - \Lambda_2)], \quad (15)$$

$$\delta\tilde{\Lambda} = \frac{1}{2} [\sqrt{1 - 4\eta} (1 - \frac{13272}{1319}\eta + \frac{8944}{1319}\eta^2) (\Lambda_1 + \Lambda_2) + (1 - \frac{15910}{1319}\eta + \frac{32850}{1319}\eta^2 + \frac{3380}{1319}\eta^3) (\Lambda_1 - \Lambda_2)] \quad (16)$$

We use different EoS models as described in Sec. II to relate each NS mass (m_1, m_2) to the corresponding tidal deformability parameter (Λ_1, Λ_2). The M - Λ relation is obtained for each EoS by solving the Tolman-Oppenheimer-Volkov (TOV) equations, together with the differential equations for perturbed relativistic stars described by [57, 58]. In the case where a phase transition appears in the NS, additional terms due to jumps in thermodynamic quantities must be taken into account. To do this, we follow the approach by [59].

For each EoS, we assume fixed values for the spins and inclination $\chi_1 = 0.01$, $\chi_2 = 0.005$, $\iota = 45^\circ$ and inject a series of events into `GWBENCH`, with chosen values for the chirp mass \mathcal{M}_c , the mass ratio $q = m_2/m_1$ and the luminosity distance \mathcal{D}_L . $\tilde{\Lambda}$ and $\delta\tilde{\Lambda}$ are deduced from the M - Λ relation for the specific EoS considered and Eqs. (15), (16). The detector features are those of the

projected third-generation ground-based ones: triangle-shaped Einstein Telescope [ET, see 16] and two Cosmic Explorer detectors [CE, see 18]. Details about their power spectral densities (PSD) and exact projected locations are given in Appendix C of [52]. `GWBENCH` then returns estimates of measurement errors in the parameters of our waveform models. These estimates shall be used in the next sections, in particular for the case of $\tilde{\Lambda}$. Concerning $\delta\tilde{\Lambda}$, this parameter only enters at the sixth post-Newtonian (6 PN) order in the waveform, meaning, it is subdominant with respect to the leading-order 5 PN tidal correction [56]. For this reason, it is not possible to obtain error-bound estimates of $\delta\tilde{\Lambda}$ within our approach; it can be however estimated using EoS-independent relations [60].

IV. BAYESIAN FRAMEWORK

We use a Bayesian framework to quantify the compatibility of a simulated observation between a purely nucleonic and a hybrid (nucleons+quarks) neutron star core. For the different EoS, we employed the techniques outlined in Secs. IIA 1 and IIB based on [61, 62]. To build the prior for the nucleonic metamodel, 12 NMPs corresponding to uniform matter were varied randomly with a constant probability distribution over a wide domain. Since the expansion in Eq. (2) is truncated at the fourth order, it is necessary to use different $Q_{(sat,sym)}$ and $Z_{(sat,sym)}$ below and above n_{sat} to increase the reliability of the expansion over a large density range. In particular, it makes the EoS free of any fictitious correlations between observables connected more to the low and high-density regimes, respectively. Since these high-order NMPs have no contribution in Eq. (1) at n_{sat} , this way of choosing different values for coefficients of the same order in the expansion does not induce any discontinuity in the energy, pressure or sound speed. This leads to a total of 16 parameters for the nucleonic EoS.

For the hybrid EoSs, containing nucleons and quarks, we obtained three families namely ‘‘PT03’’, ‘‘PT04’’ and ‘‘PT05’’ based on the density n_t at the onset of the nucleon-quark transition fixed to 0.3, 0.4 and 0.5 fm⁻³, respectively. For all hybrid models, the width of the plateau $\Delta\varepsilon$ is chosen by imposing a random value for the lowest baryon density in the quark phase varying between n_t and $1.5n_t$. Finally, the squared sound speed c_s^2 is randomly varied between 0.1 and 0.9 c^2 , where c is the speed of light. These large variations were used to cover a large space in the $p(\varepsilon)$ plane by our hybrid models. It should be kept in mind, that a constant sound speed description can of course not recover a more complicated behaviour inherent to more sophisticated microscopic models for quark matter, see e.g. [63–70], but the chosen range should be able to enclose most models such that we consider our assumptions as very conservative.

It is quite important to mention here the particular motivation to keep n_t fixed at distinct values, rather than

varying it randomly within a range, too. Since a random n_t would only introduce further uncertainty on top of the nucleonic EoS, the fully nucleonic metamodel would be systematically preferred irrespective of any observation. We thus target to identify the signature of nucleon-quark phase transition, based on its early or late appearance in terms of density.

A. Obtaining an informed prior

On the whole, to perform the Bayesian analysis we have used 16 parameters ($N_p = 16$) for the nucleonic metamodel and 19 parameters ($N_p = 19$) for “PT03”, “PT04” and “PT05” hybrid metamodels. The uninformed prior distribution $P_{prior}(\mathbf{X}) = \prod_{k=1}^{N_p} P_k(X_k)$ of the parameter set $\mathbf{X} \equiv \{X_k, k = 1, \dots, N_p\}$ is obtained with a flat uncorrelated distribution $P_k(X_k)$. To obtain a prior informed by different observations, the probability of each model is then conditioned by the likelihood models of the AME2016 mass evaluation [49], low density constraints on SNM and PNM obtained from theoretical χ -EFT calculations [71], constraint from the observed maximum mass of NS [7, 8] and constraints on the joint tidal deformability $\tilde{\Lambda}$ of the GW170817 event [72] as

$$P_{prior}^{\text{informed}}(\mathbf{X}) = P(\mathbf{X}|\mathbf{c}) = \mathcal{N} \cdot P_{AME2016}(\mathbf{X}) P_{\chi\text{-EFT}}(\mathbf{X}) \times P_{M_{max}}(\mathbf{X}) P_{GW170817}(\mathbf{X}) \prod_k P(c_k|\mathbf{X}). \quad (17)$$

Here, \mathcal{N} is a normalization constant. The AME2016 filter is obtained as

$$P_{AME2016}(\mathbf{X}) \propto \omega_{AME} e^{-\chi_{AME}^2(\mathbf{X})/2}, \quad (18)$$

where, $\omega_{AME} = 0$ or 1 depending on the meaningful reproduction or not, of the whole AME2016 mass table [49], respectively. The objective function for the AME2016 mass table is given by

$$\chi_{AME}^2(\mathbf{X}) = \frac{1}{N} \sum_n \frac{\left((B/A)_{CLDM}^{(n)}(\mathbf{X}) - (B/A)_{AME}^{(n)} \right)^2}{\sigma_{BE}^2} \quad (19)$$

with $N = 2408$ and the adopted error $\sigma_{BE} = 0.04$ MeV. The probability for the χ -EFT pass-band type filter based on the constraints on SNM and PNM between $n = 0.02$ and 0.2 fm^{-3} is obtained from the theoretical calculation in [71] as,

$$P_{\chi\text{-EFT}}(\mathbf{X}) \propto \omega_{\chi\text{-EFT}}(\mathbf{X}), \quad (20)$$

where, $\omega_{\chi\text{-EFT}}(\mathbf{X}) = 0$ or 1, depending on SNM and PNM corresponding to \mathbf{X} passing through the whole range or not. This theoretical band was obtained from the 90% confidence interval, which we have increased by 5% on the edges to interpret it as a 2σ band. The probability assigned to each model due to observed maximum

mass $M_{max}^{obs} = 2.01 \pm 0.04 M_\odot$ [8], following a cumulative probability distribution, is given by

$$P_{M_{max}}(\mathbf{X}) = \frac{1}{0.04\sqrt{2\pi}} \int_0^{M_{max}(\mathbf{X})/M_\odot} e^{-\frac{(x-2.01)^2}{2 \times 0.04^2}} dx \quad (21)$$

The effect of the joint tidal deformability $\tilde{\Lambda}$ observed during the GW170817 event [72] on the different metamodels and hybrid metamodels are obtained from a two dimensional probability distribution $P_{GW170817}(\tilde{\Lambda}(q), q)$ as,

$$P_{GW170817}(\mathbf{X}) = \sum_i P_{GW170817}(\tilde{\Lambda}(q^{(i)}), q^{(i)}). \quad (22)$$

Here, we have assumed a constant $\mathcal{M}_c = 1.186 M_\odot$ due to the small uncertainty in the observed chirp mass. For each model \mathbf{X} , we sampled $q \in [0.73, 1]$ and interpolated the probabilities from the two dimensional distribution $P_{GW170817}(\tilde{\Lambda}(q), q)$ to perform the sum in Eq. (22).

Once the informed prior probability for each model is obtained, the corresponding probability distribution for the observables is obtained by marginalizing over the range of parameters $\mathbf{X} \in [\mathbf{X}_{min}, \mathbf{X}_{max}]$ as,

$$P_{prior}^{\text{informed}}(Y) = \prod_{k=1}^N \int_{X_k^{min}}^{X_k^{max}} dX_k P_{prior}^{\text{informed}}(\mathbf{X}) \delta(Y - Y(\mathbf{X})) \quad (23)$$

B. Confronting the models with simulated “observations”

To identify the signature of a phase transition in the gravitational wave signal from a BNS coalescence, we examine the compatibility of the purely nucleonic metamodel and the hybrid metamodels subjected to a given event. As described in section III, we consider a hypothetical BNS coalescing event specified by $\{\mathcal{M}_c^0, q_0, \tilde{\Lambda}_0\}$, where \mathcal{M}_c is the chirp mass, $q = m_2/m_1$ the mass ratio, and $\tilde{\Lambda}$ the tidal deformability. To determine $\tilde{\Lambda}_0(\mathcal{M}_c^0, q_0)$ we use a specific EoS model from one of the hybrid metamodel families. Given the characteristics of the detector, the distance (\mathcal{D}_L) and the sky location, we then calculate the interferometer response to this event via GWBENCH using the aforementioned EoS model. This gives us a posterior experimental distribution $p_{GW}^0(\mathcal{M}_c, q, \tilde{\Lambda})$, as well as the marginalized distributions $p_{GW}^0(\mathcal{M}_c)$, $p_{GW}^0(q)$, $p_{GW}^0(\tilde{\Lambda})$, that of course will implicitly depend on the choice \mathcal{M}_c^0, q_0 , together with the detector characteristics. Since the chirp mass is very well measured, we will always assume $p_{GW}^0(\mathcal{M}_c) = \delta(\mathcal{M}_c - \mathcal{M}_c^0)$.

Once an “observation” is simulated with a model from the hybrid metamodel class, we want to confront the tidal polarizability measurement $p_{GW}^0(\tilde{\Lambda})$ with the nucleonic hypothesis. To make the comparison, in principle, we could calculate

$$p_{meta}^{(0)}(\tilde{\Lambda}) \equiv p(\tilde{\Lambda} | meta, BI = \mathcal{M}_c^0, q_0), \quad (24)$$

where *meta* denotes the nucleonic metamodel, and *BI* the background information. However, if we consider that $p_{GW}^0(\tilde{\Lambda})$ corresponds to a true measurement, \mathcal{M}_c^0 and q_0 are not known exactly, but only as a distribution $p_{GW}^0(\mathcal{M}_c, q)$. Thus, the only quantity we can meaningfully compare to $p_{GW}^0(\tilde{\Lambda})$ is the distribution given by,

$$p_{meta}^{(1)}(\tilde{\Lambda}) \equiv p(\tilde{\Lambda} | meta, BI = \mathcal{M}_c^0, p_{GW}^0(q)). \quad (25)$$

Imposing to the nucleonic metamodel a q distribution identical to the one hypothetically extracted from the ‘‘observation’’ clearly gives a distribution more spread than $p_{meta}^{(0)}(\tilde{\Lambda})$, which is the only one that we will be able to compare to the observation. A similar probability distribution corresponding to the hybrid metamodel is expressed as

$$p_{PT}^{(1)}(\tilde{\Lambda}) \equiv p(\tilde{\Lambda} | PT, BI = \mathcal{M}_c^0, p_{GW}^0(q)), \quad (26)$$

where *PT* signifies hybrid metamodels containing a first-order hadron-quark phase transition.

In the end, to distinguish the compatibility of observation with the nucleonic metamodel and the hybrid metamodels, one can resort to evidence in terms of Bayes factors. Given an event, the Bayes factor can be defined as a function of $\tilde{\Lambda}$ as

$$B_{PT,meta}(\tilde{\Lambda}) = \frac{p_{PT}^{(1)}(\tilde{\Lambda})}{p_{meta}^{(1)}(\tilde{\Lambda})}, \quad (27)$$

$$B_{meta,PT}(\tilde{\Lambda}) = \frac{1}{B_{PT,meta}(\tilde{\Lambda})}. \quad (28)$$

The average Bayes factors associated to the simulated observation $p_{GW}^0(\tilde{\Lambda})$ is specified as

$$\log(\langle B \rangle_{PT,meta}^{\mathcal{M}_c^0, q_0}) = \int d\tilde{\Lambda} p_{GW}^0(\tilde{\Lambda}) \log \left[\frac{p_{PT}^{(1)}(\tilde{\Lambda})}{p_{meta}^{(1)}(\tilde{\Lambda})} \right] \quad (29)$$

$$\log(\langle B \rangle_{meta,PT}^{\mathcal{M}_c^0, q_0}) = \int d\tilde{\Lambda} p_{GW}^0(\tilde{\Lambda}) \log \left[\frac{p_{meta}^{(1)}(\tilde{\Lambda})}{p_{PT}^{(1)}(\tilde{\Lambda})} \right] \quad (30)$$

V. RESULTS

A. Hybrid metamodels

To set the stage for confronting simulated observations with families of EoS with or without a PT to quark matter, we need to obtain an informed prior as described by Eq.(17) and (23). Distributions of these informed priors for different nuclear matter parameters of the nucleonic metamodeling can be found in [61, 62] as posteriors. In Fig. 1 we display the distributions of the sound speed parameter c_s^2 in panel (a) and width of the plateau $\Delta\varepsilon$ in panel (b) for the new class of hybrid metamodels PT03, PT04 and PT05, as described in Sec. II A 2 and IV. To highlight the impact of the astrophysical constraints like the observed M_{max} or $\tilde{\Lambda}$ from GW170817 on the hybrid

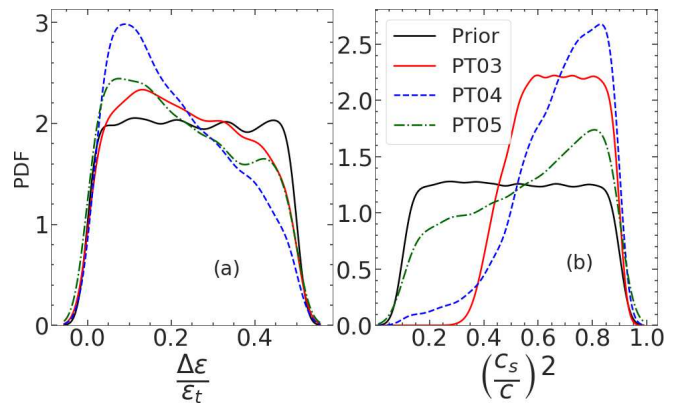


FIG. 1. Informed prior distribution of the width of plateau $\Delta\varepsilon$ in units of energy density at transition ε_t and squared sound speed c_s^2 in units of speed of light c with phase transitions at 0.3, 0.4 and 0.5 fm^{-3} for hybrid metamodels PT03, PT04 and PT05, respectively (see text for details).

metamodels, we display the prior distributions of $\Delta\varepsilon$ and c_s^2 in Fig. 1, too. For PT03, models with small values of c_s^2 ($< 0.4c^2$) get suppressed significantly, but the rest still remain uniformly distributed. The hybrid metamodel PT04 clearly prefers to have larger c_s^2 , which somewhat evens out for PT05. The distributions of $\Delta\varepsilon$ for different hybrid metamodels obtain crests at smaller values (*i.e.* no first-order PT) compared to the uninformed flat prior.

In Fig. 2(a) we display the EoS of the nucleonic metamodel along with hybrid metamodels PT03, PT04 and PT05 in a 1σ confidence interval. We remind that these EoS posteriors are consistent with various observational constraints as described in section IV A. One can observe that with increasing transition density n_t from nucleonic to quark matter, the overall region explored in the p - n plane increases. An early phase transition requires a very stiff behaviour of the quark phase, such as to meet the $2M_\odot$ constraint. On the other hand, relatively softer behaviours, corresponding to lower values of the c_s^2 parameter, are allowed if the quark phase emerges at higher densities. This is consistent with the distribution of c_s^2 displayed in Fig. 1(b).

In order to simulate hypothetical observations within the Fisher formalism, one needs specific injection EoS models. We chose different injection models for PT03, PT04 and PT05 guided by the 1σ boundaries displayed in Fig. 2(a). The representative injection EoS are displayed in Fig. 2(b) for PT03, PT04 and PT05 hybrid metamodels, respectively. Except for the plateau region, each individual injection model follows the 16%, 33%, 50%, 67% and 84% quantiles of the corresponding posteriors from the bottom to the top (or right to left), respectively. We follow the nomenclature for the injection models obtained at the 16% and 84% quantiles as ‘‘ 1σ -lower’’ and ‘‘ 1σ -upper’’ models (*c.f.* Figs 4-7) of the corresponding hybrid metamodel classes *i.e.* PT03, PT04 and PT05, respectively.

In Fig. 3 we plot the two dimensional informed prior

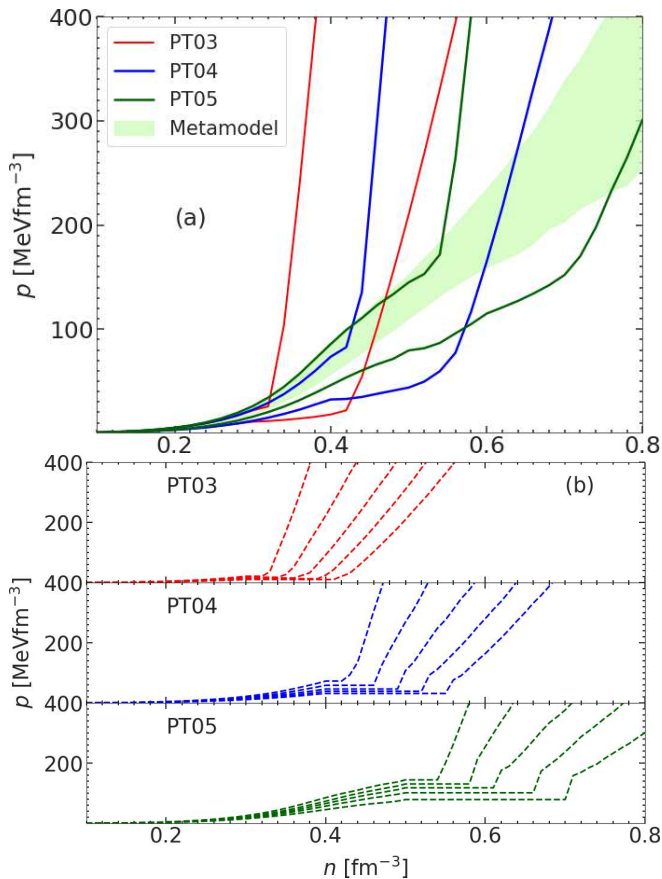


FIG. 2. (a): Pressure at β -equilibrium as a function of number density n at the 1σ confidence interval obtained for nucleonic Metamodel and hybrid metamodels PT03, PT04 and PT05; (b): Injection models with first-order phase transitions based on the intervals given in panel (a) obtained for simulated “observations” using GWBENCH (see text for more details).

distribution for M - R (panel(a)) and Λ - M (panel (b)) relations of NSs using nucleonic and different hybrid metamodels. Introducing a first-order hadron-quark phase transition (c.f. Fig. 2(a)) in the hybrid metamodels and the further requirements from various astrophysical constraints categorically soften the EoS. However, this does not systematically shift the hybrid metamodels to explore smaller R or Λ at a given M , with incremental n_t *i.e.* from 0.3 to 0.5 fm $^{-3}$ due to the behaviour of the nucleonic model in between the different transition densities. Beyond $1.2 M_\odot$, PT03 and the nucleonic metamodel explore almost complementary regions in the M - R and Λ - M planes at the $1 - \sigma$ level. The overlap regions increase significantly between PT04 and nucleonic Metamodel for both M - R and Λ - M . At larger masses ($> 1.5 M_\odot$) PT04 also explores smaller R and Λ compared to the other families of hybrid metamodels considered in this work. PT05 almost engulfs the nucleonic metamodel, additionally exploring smaller values of R and Λ at larger masses ($> 1.7 M_\odot$). Essentially these differences in Λ displayed in Fig. 3 are manifested in the joint tidal deformability

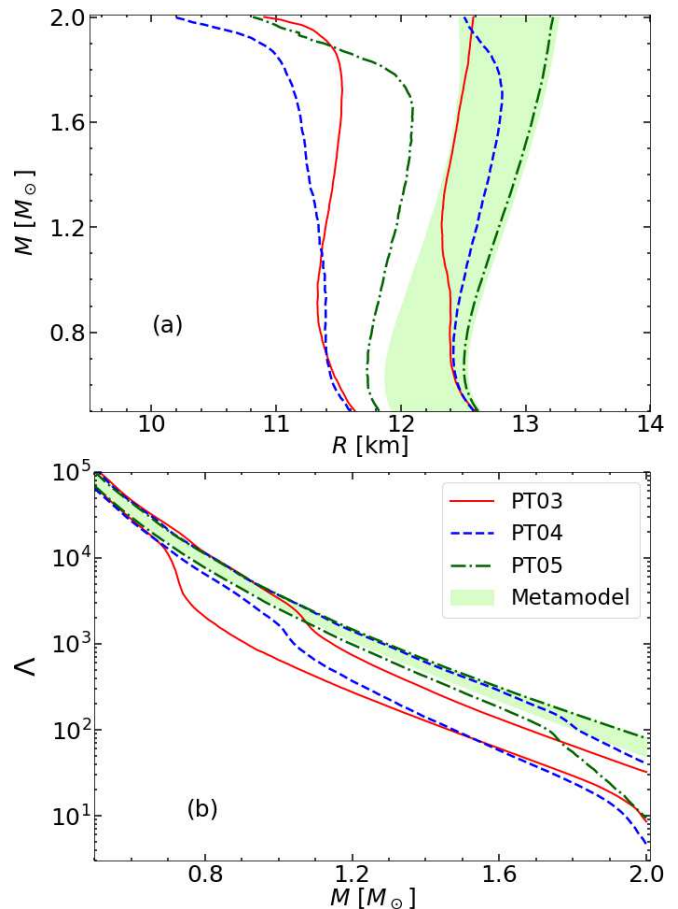


FIG. 3. M - R and Λ - M relations at 1σ confidence interval obtained for nucleonic Metamodel and hybrid metamodels PT03, PT04 and PT05.

TABLE I. Different GWBENCH injection parameters which were varied are listed. For all of them, $\chi_1 = 0.01$, $\chi_2 = 0.005$, $\iota = 45^\circ$ were kept fixed. $\tilde{\Lambda}$ and $\delta\tilde{\Lambda}$ were fixed by the underlying injection models depicted in Fig. 2(b).

Parameter	Range	Step-size
$\mathcal{M}_c^0 (M_\odot)$	1.1 - 1.46	0.045
$q_0 = \frac{m_2}{m_1}$	0.79 - 0.99	0.05
\mathcal{D}_L (Mpc)	22, 120, 221, 326, 433, 544, 657, 772, 891, 1012	

$\tilde{\Lambda}$, which is explored in detail in the next section.

B. Simulated observations

As an exploratory study, we start by considering single events, choosing at each time specific values of chirp mass \mathcal{M}_c^0 , mass ratio q_0 , and luminosity distance \mathcal{D}_L keeping the remaining parameters defining a BNS coalescence, *viz.* spin $\vec{\chi}$ of the constituents, inclination ι etc. fixed. Altogether, we considered 9 values of \mathcal{M}_c^0 , 5 values of

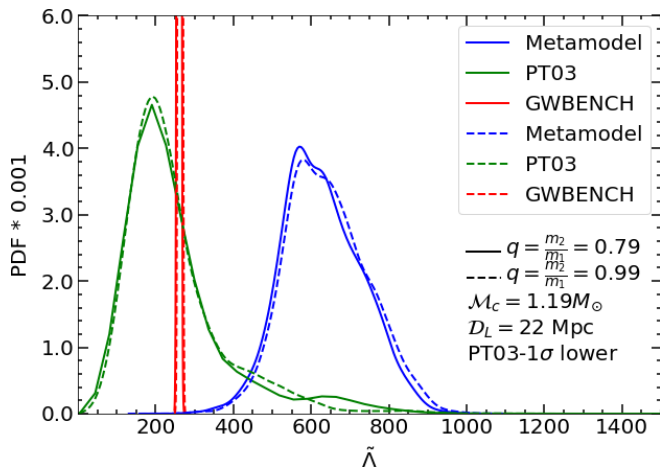


FIG. 4. Probability distribution functions of joint tidal deformability $\tilde{\Lambda}$ in nucleonic Metamodel, hybrid metamodel PT03 and GWBENCH for mass ratio $q = 0.79$ (solid) and $q = 0.99$ (dashed) obtained using PT03-1 σ -lower injection model, $\mathcal{M}_c = 1.19 M_\odot$ and $\mathcal{D}_L = 22$ Mpc.

q_0 situated at 10 different \mathcal{D}_L as outlined in Table. I. The response of the Fisher matrix formalism for a chosen EoS was tested for these 450 assumed events with equal probability. 5 different hybrid EoSs from each of the PT03, PT04 and PT05 families were used for this purpose, which are displayed explicitly in Fig. 2(b). Note that we use the notation \mathcal{M}_c and q instead of \mathcal{M}_c^0 and q_0 , from here onward, respectively. This is just for simplicity.

We want to emphasize here that assumptions about the chosen events, and how they are distributed in the sky can affect the quantitative outcomes we are going to demonstrate in this section. However, the methodology proposed here can be used to incorporate models of neutron star mass distributions, see e.g. [73]. We leave it as a future study.

Before diving into the calculation of Bayes factors as demonstrated in Eqs. (29)-(30), let us first analyze the premises chosen in the different astrophysical parameters and EoS modelling for the present endeavour. To this aim, we compare systematically the probability distribution functions (PDFs) of $\tilde{\Lambda}$ of BNS merging events that enter in Eqs. (29)-(30), *i.e.*, $p_{GW}^0(\tilde{\Lambda})$, $p_{PT}^{(1)}(\tilde{\Lambda})$, and $p_{meta}^{(1)}(\tilde{\Lambda})$ calculated from GWBENCH, hybrid and nucleonic metamodels, respectively, changing one variable at a time, keeping the rest fixed. In Fig. 4, we plot the PDFs of $\tilde{\Lambda}$ calculated from nucleonic metamodel (blue), hybrid metamodel PT03 (green) and GWBENCH (red) for two extreme mass ratios $q = 0.79$ (solid lines) and $q = 0.99$ (dashed lines) considered in the present calculation. In both cases, $\mathcal{M}_c = 1.19 M_\odot$, $\mathcal{D}_L = 22$ Mpc were kept fixed and the same injection model PT03-1 σ -lower was used in GWBENCH. The differences due to the variation in q are almost negligible. In the case of a very close detection shown in Fig. 4, the theoretical uncertainties clearly prime over the observational ones. In spite

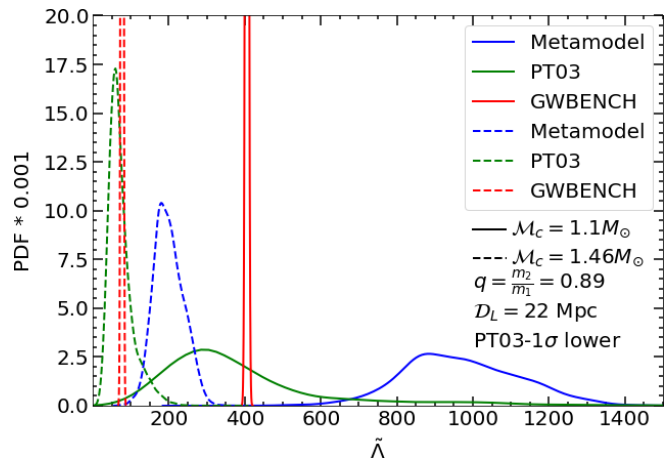


FIG. 5. The same as Fig. 4 but for $\mathcal{M}_c = 1.1 M_\odot$ (solid) and $\mathcal{M}_c = 1.46 M_\odot$ (dashed) using PT03-1 σ -lower injection model, $q = 0.89$ and $\mathcal{D}_L = 22$ Mpc.

of those large uncertainties, the two theoretical distributions only marginally overlap. The Bayes factors calculated for $q = 0.79$ and $q = 0.99$ as depicted in Fig. 4 using Eq. (29) turned out to be $\log(\langle B \rangle_{PT03,meta}^{1.19 M_\odot, 0.79}) = 2.15$ and $\log(\langle B \rangle_{PT03,meta}^{1.19 M_\odot, 0.99}) = 1.56$, respectively. We have observed that the quantitative values of the Bayes factors demonstrated here can further increase if a larger \mathcal{M}_c is chosen.

This is exactly what is analyzed in Fig. 5, where we show the PDFs of $\tilde{\Lambda}$ calculated from the nucleonic metamodel (blue) and one of its hybrid counterparts PT03 (green) along with GWBENCH (red) for two extreme cases of chirp masses $\mathcal{M}_c = 1.1 M_\odot$ (solid lines) and $\mathcal{M}_c = 1.46 M_\odot$ (dashed lines) considered in the present calculation. The same injection model PT03-1 σ -lower was used in this study as in Fig. 4. The mass ratio q and luminosity distance \mathcal{D}_L was kept fixed at 0.89 and 22 Mpc, respectively. Clearly, the difference in \mathcal{M}_c results in a change in the position of the peaks of the PDFs as well as their widths. The particular scenario depicted in Fig. 5 for $\mathcal{M}_c = 1.1 M_\odot$ and $\mathcal{M}_c = 1.46 M_\odot$ results in a big difference in the Bayes factors, $\log(\langle B \rangle_{PT03,meta}^{1.1 M_\odot, 0.89}) = 1.54$ and $\log(\langle B \rangle_{PT03,meta}^{1.46 M_\odot, 0.89}) = 3.22$, respectively. In general, the effect of \mathcal{M}_c is found to be much stronger in the Bayes factor compared to the mass ratio q , if the rest of the variables are kept fixed. Identification of the first-order PT will thus be more probable from the future observations for events with larger \mathcal{M}_c 's.

We lay our focus on the impact of injection models on the PDFs of $\tilde{\Lambda}$ in Fig. 6. Like the analysis done in Figs. 4 and 5, there is no exact guide to choose two extreme injection models from the ones outlined in Fig. 2(b). Keeping an eye on Fig. 2(a), we choose PT03-1 σ -lower and PT05-1 σ -upper with the idea that they have the least and maximum overlap with the nucleonic meta-

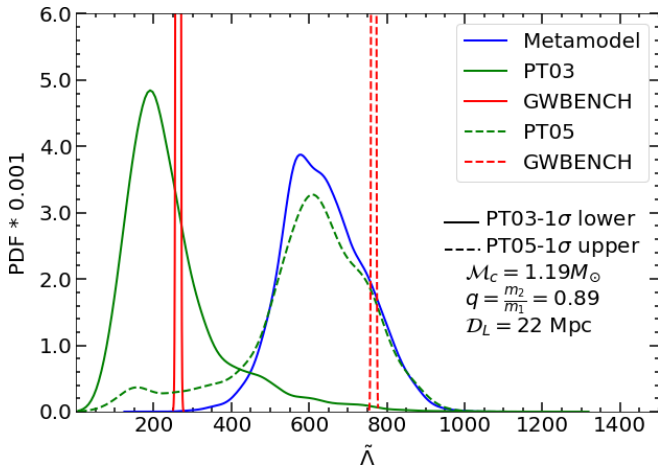


FIG. 6. The same as Fig. 4 but for injection models PT03-1 σ -lower (solid) and PT05-1 σ -upper (dashed) using $\mathcal{M}_c = 1.19 M_\odot$, $q = 0.89$ and $\mathcal{D}_L = 22$ Mpc.

model, respectively. PDFs of $\tilde{\lambda}$ obtained using PT03-1 σ -lower (solid lines) and PT05-1 σ -upper (dashed lines) are displayed in Fig. 6 for the nucleonic metamodel (blue), hybrid metamodels (green) and GWBENCH (red). One should note that, depending on the injection models we display the corresponding hybrid metamodels PT03 and PT05, respectively. Since the underlying astrophysical event is the same with $\mathcal{M}_c = 1.19 M_\odot$, $q = 0.89$ and $\mathcal{D}_L = 22$ Mpc, the PDF of $\tilde{\lambda}$ obtained with nucleonic Metamodel appears as a common one for both the injection models. The Bayes factors for the cases considered in Fig. 6 turn out to be $\log(\langle B \rangle_{PT03,meta}^{1.19 M_\odot, 0.89}) = 1.79$ and $\log(\langle B \rangle_{PT05,meta}^{1.19 M_\odot, 0.89}) = 0.02$ for PT03-1 σ -lower and PT05-1 σ -upper, respectively. This gives already an indication that identifying an early hadron-quark first-order PT will be more probable than a later one from future gravitational wave signals.

Depending on how far one BNS merger event takes place, the signal-to-noise ratio (SNR) recorded in gravitational wave interferometers can vary a lot. We have analyzed, to this aim, an event with $\mathcal{M}_c = 1.19 M_\odot$, $q = 0.89$ simulated using PT03-1 σ -lower injection model at luminosity distances $\mathcal{D}_L = 22$ Mpc (solid lines) and $\mathcal{D}_L = 1012$ Mpc (dashed lines) in Fig. 7. The PDFs of $\tilde{\lambda}$ corresponding to the nucleonic metamodel, hybrid metamodel PT03 and GWBENCH are displayed in blue, green and red, respectively. The broadening of the PDFs from the case with $\mathcal{D}_L = 22$ Mpc to the case with $\mathcal{D}_L = 1012$ Mpc is clearly visible, which eventually affects the calculation of Bayes factors using Eq. (29). For $\mathcal{D}_L = 22$ Mpc, the Bayes factor is $\log(\langle B \rangle_{PT03,meta}^{1.19 M_\odot, 0.89}) = 1.79$ (same as the one obtained from the solid lines in Fig. 6); for $\mathcal{D}_L = 1012$ Mpc the Bayes factor becomes $\log(\langle B \rangle_{PT03,meta}^{1.19 M_\odot, 0.89}) = 0.76$. Even though in this particular case depicted in Fig. 7, there is a clear hint of

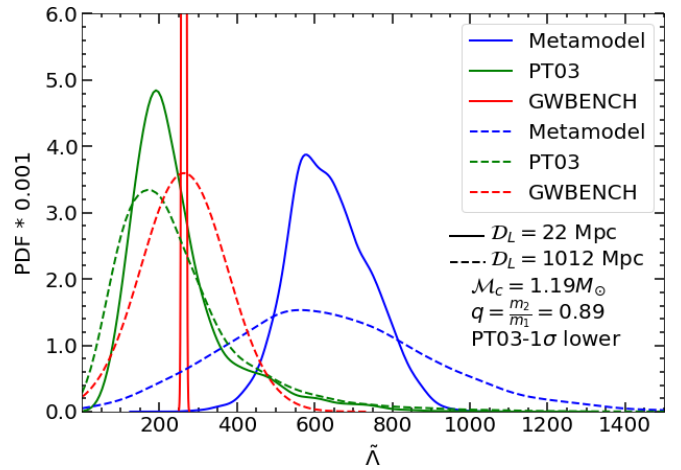


FIG. 7. The same as Fig. 4 but for $\mathcal{D}_L = 22$ Mpc (solid) and $\mathcal{D}_L = 1012$ Mpc (dashed) using PT03-1 σ -lower injection model, $\mathcal{M}_c = 1.19 M_\odot$ and $q = 0.89$.

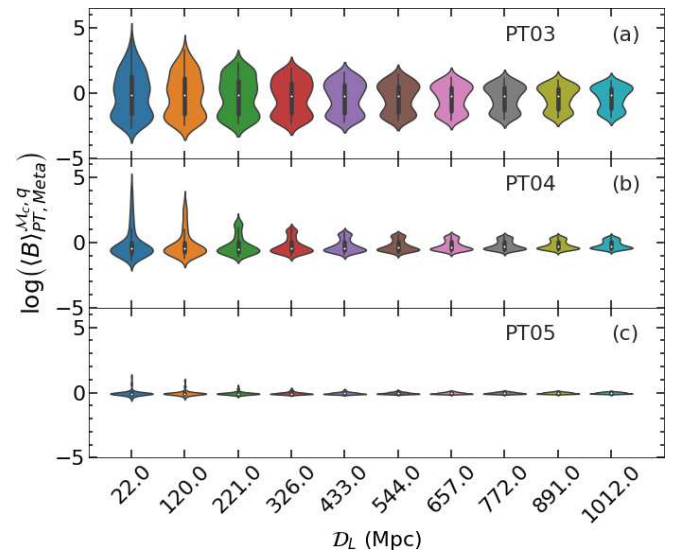


FIG. 8. Average Bayes factor as a function of luminosity distance \mathcal{D}_L for different injection models, averaged over the respective class of hybrid metamodels using Eq. (29). The distributions come from the variation in q and \mathcal{M}_c considered in the present calculation (see Table I).

hybrid metamodel to be preferred over the nucleonic one, the evidence is not significant enough, even if we suppose an early phase transition.

To have the global picture of the PT detectability, we plot the Bayes factors at different luminosity distances \mathcal{D}_L comparing PT03, PT04 and PT05 against the nucleonic metamodel in panels (a), (b) and (c) of Fig. 8, respectively. In each panel, at a given \mathcal{D}_L , the variation in $\log(\langle B \rangle_{PT,meta}^{M_c, q})$ comes from the variation in \mathcal{M}_c , q and injections models. Since we are interested in identifying the notion of a phase transition, high values of $\log(\langle B \rangle_{PT,meta}^{M_c, q}) \geq 1 - 2$ is our primary concern [74].

From Fig. 8(c) it is evident that the existence of a first-order transition at around 0.5 fm^{-3} ($\sim 3n_{sat}$) can't be identified from a single gravitational wave signal with third generation interferometers. In Fig. 8(a) the other extreme case considered in the present calculation, *i.e.*, a phase transition at 0.3 fm^{-3} ($\sim 2n_{sat}$) seems to be a viable situation that can be identified particularly with high confidence at distances less than 300 Mpc. The highest positive values of $\log \left(\langle B \rangle_{PT,meta}^{\mathcal{M}_c,q} \right)$ at almost all distances are associated with larger \mathcal{M}_c 's obtained using injection models with lower quantiles (see Fig. 2(b) and the corresponding discussion). It seems from Fig. 8(b) that only for a small percentage of events at low luminosity distances ($\mathcal{D}_L \lesssim 100 \text{ Mpc}$) a phase transition can be identified if nature prefers to have it at $\sim 0.4 \text{ fm}^{-3}$. Particularly, at $\mathcal{D}_L = 22 \text{ Mpc}$ the high $\log \left(\langle B \rangle_{PT,meta}^{\mathcal{M}_c,q} \right)$ values correspond to $\mathcal{M}_c > 1.4 M_\odot$ obtained with PT04-1 σ -lower injection model. We expect that the detectability of a first order phase transition reported in the present study will be largely improved by considering multiple detections, as expected by the future Einstein Telescope. To this aim, we plan to study the evolution of the Bayes factors as a function of the number of detections, by including realistic population distributions.

VI. SUMMARY AND DISCUSSION

In summary, we have presented an updated metamodelling technique for the EoS in neutron star matter including potential first-order hadron-quark phase transitions. The hadronic core is assumed to have only nucleons and leptons up to a specified density. The EoS for the nucleonic core is obtained by an optimized expansion in number density truncated at fourth order following [40]. The crust EoS and composition are subsequently extracted with a unified approach in the spherical Wigner-Seitz approximation. The extension of the EoS modelling in the quark core is done with the constant sound speed model, without dwelling on the microscopic composition.

Three classes of hybrid (nucleon + quark) metamodels PT03, PT04 and PT05 named after the density corresponding to the hadron-quark phase transition, *i.e.*, 0.3, 0.4 and 0.5 fm^{-3} , respectively, were generated. These hybrid metamodels were already made compliant with different nuclear physics and astrophysics constraints within the Bayesian paradigm. Using these hybrid and nucleonic posteriors, we proposed a framework based on Bayes factors to discriminate a possible sign of phase transition from future gravitational wave signals generated by BNS mergers. To simulate future observational signals, we used the Fisher matrix formalism employing the publicly available tool GWBENCH [52] that simulates the gravitational wave signal using the TaylorF2 + tidal waveform templates and includes the detector features of the pro-

jected third-generation ground-based interferometers. We considered a single detection, and compared different chosen cases corresponding to different masses of NSs, located at different distances, and using injection models which include first-order phase transition. In particular, these hybrid injection models were constructed out of PT03, PT04 and PT05 1 σ posteriors, which are already informed by different physical constraints. We have critically assessed the impact of diversified variables in the discrimination of a phase transition signature through the Bayes factors.

We have found that the mass ratio of the constituents of a BNS merger does not play a significant role in the magnitude of the Bayes factors. Overall, higher chirp mass, smaller luminosity distances and early phase transition with strong first-order effect can facilitate a possible identification of phase transition from future gravitational wave signals. Further, we have found that if nature prefers to have a phase transition at higher densities ($\gtrsim 3n_{sat}$), it is most likely to be masked, since it would be possible to explain that with an EoS model without phase transition.

This study is directed mostly towards structuring a framework to look for the signatures of phase transition in future gravitational wave signals generated by BNS mergers. A further study incorporating realistic population models is needed to estimate the effect of multiple detections. It is also going to be important to incorporate microscopic modelling in the quark phase to extract further physical information regarding composition at high densities. We leave these ventures for future studies.

VII. ACKNOWLEDGEMENTS

We would like to thank Anthea Fantina for enlightening discussions as well as a careful reading of the manuscript, and Ssohrab Borhanian for fruitful exchanges and support on gwbench. This work has been partially supported by the IN2P3 Master Project NewMAC and the AAPG2022 ANR project GWsNS. The authors gratefully acknowledge the Italian Istituto Nazionale de Fisica Nucleare (INFN), the French Centre National de la Recherche Scientifique (CNRS) and the Netherlands Organization for Scientific Research for the construction and operation of the Virgo detector and the creation and support of the EGO consortium.

VIII. DATA AVAILABILITY

No new data were generated in support of this research. The numerical results and the code underlying this article will be shared upon reasonable request to the authors.

-
- [1] P. Haensel, A.Y. Potekhin, and D.G. Yakovlev. *Neutron Stars 1: Equation of State and Structure*. Astrophysics and Space Science Library. Springer New York, 2007.
- [2] Fiorella G. Burgio and Anthea F. Fantina. Nuclear Equation of state for Compact Stars and Supernovae. *Astrophys. Space Sci. Libr.*, 457:255–335, 2018.
- [3] M. Oertel, M. Hempel, T. Klöhn, and S. Typel. Equations of state for supernovae and compact stars. *Rev. Mod. Phys.*, 89(1):015007, 2017.
- [4] J. M. Lattimer. Impact of GW170817 for the nuclear physics of the EOS and the r-process. *Annals Phys.*, 411:167963, 2019.
- [5] N. Chamel and P. Haensel. Physics of Neutron Star Crusts. *Living Rev. Rel.*, 11:10, 2008.
- [6] Adriana R. Raduta. Equations of state for hot neutron stars-II. The role of exotic particle degrees of freedom. *Eur. Phys. J. A*, 58(6):115, 2022.
- [7] Paul Demorest, Tim Pennucci, Scott Ransom, Mallory Roberts, and Jason Hessels. Shapiro Delay Measurement of A Two Solar Mass Neutron Star. *Nature*, 467:1081–1083, 2010.
- [8] John Antoniadis et al. A Massive Pulsar in a Compact Relativistic Binary. *Science*, 340:6131, 2013.
- [9] Emmanuel Fonseca et al. The NANOGrav Nine-year Data Set: Mass and Geometric Measurements of Binary Millisecond Pulsars. *Astrophys. J.*, 832(2):167, 2016.
- [10] H. Thankful Cromartie et al. Relativistic Shapiro delay measurements of an extremely massive millisecond pulsar. *Nature Astronomy*, page 439, Sep 2019.
- [11] M. C. Miller et al. The Radius of PSR J0740+6620 from NICER and XMM-Newton Data. *Astrophys. J. Lett.*, 918(2):L28, 2021.
- [12] Thomas E. Riley et al. A NICER View of the Massive Pulsar PSR J0740+6620 Informed by Radio Timing and XMM-Newton Spectroscopy. *Astrophys. J. Lett.*, 918(2):L27, 2021.
- [13] M. C. Miller et al. PSR J0030+0451 Mass and Radius from NICER Data and Implications for the Properties of Neutron Star Matter. *Astrophys. J. Lett.*, 887(1):L24, 2019.
- [14] Thomas E. Riley et al. A NICER View of PSR J0030+0451: Millisecond Pulsar Parameter Estimation. *Astrophys. J. Lett.*, 887(1):L21, 2019.
- [15] B. P. Abbott et al. GW170817: Observation of Gravitational Waves from a Binary Neutron Star Inspiral. *Phys. Rev. Lett.*, 119(16):161101, 2017.
- [16] M. Punturo et al. The Einstein Telescope: A third-generation gravitational wave observatory. *Class. Quant. Grav.*, 27:194002, 2010.
- [17] Michele Maggiore et al. Science Case for the Einstein Telescope. *JCAP*, 03:050, 2020.
- [18] David Reitze et al. Cosmic Explorer: The U.S. Contribution to Gravitational-Wave Astronomy beyond LIGO. *Bull. Am. Astron. Soc.*, 51(7):035, 2019.
- [19] Matthew Evans, Rana X Adhikari, Chaitanya Afle, Stefan W. Ballmer, Sylvia Biscoveanu, Ssohrab Borhanian, Duncan A. Brown, Yanbei Chen, Robert Eisenstein, Alexandra Gruson, Anuradha Gupta, Evan D. Hall, Rachael Huxford, Brittany Kamai, Rahul Kashyap, Jeff S. Kissel, Kevin Kuns, Philippe Landry, Amber Lenon, Geoffrey Lovelace, Lee McCuller, Ken K. Y. Ng, Alexander H. Nitz, Jocelyn Read, B. S. Sathyaprakash, David H. Shoemaker, Bram J. J. Slagmolen, Joshua R. Smith, Varun Srivastava, Ling Sun, Salvatore Vitale, and Rainer Weiss. A Horizon Study for Cosmic Explorer: Science, Observatories, and Community. *arXiv e-prints*, page arXiv:2109.09882, September 2021.
- [20] N. K. Glendenning, F. Weber, and S. A. Moszkowski. Neutron and hybrid stars in the derivative coupling model. *Phys. Rev. C*, 45:844–855, 1992.
- [21] Mark G. Alford. Color superconducting quark matter. *Ann. Rev. Nucl. Part. Sci.*, 51:131–160, 2001.
- [22] Michael Buballa et al. EMMI rapid reaction task force meeting on quark matter in compact stars. *J. Phys. G*, 41(12):123001, 2014.
- [23] G. A. Contrera, D. Blaschke, J. P. Carlomagno, A. G. Grunfeld, and S. Liebing. Quark-nuclear hybrid equation of state for neutron stars under modern observational constraints. *PHYSICAL REVIEW C*, 105(4), APR 27 2022.
- [24] Andreas Bauswein, Niels-Uwe F. Bastian, David B. Blaschke, Katerina Chatziioannou, James A. Clark, Tobias Fischer, and Micaela Oertel. Identifying a first-order phase transition in neutron star mergers through gravitational waves. *Phys. Rev. Lett.*, 122(6):061102, 2019.
- [25] Elias R. Most, L. Jens Papenfort, Veronica Dexheimer, Matthias Hanauske, Stefan Schramm, Horst Stöcker, and Luciano Rezzolla. Signatures of quark-hadron phase transitions in general-relativistic neutron-star mergers. *Phys. Rev. Lett.*, 122(6):061101, 2019.
- [26] Sebastian Blacker, Niels-Uwe F. Bastian, Andreas Bauswein, David B. Blaschke, Tobias Fischer, Micaela Oertel, Theodoros Soultanis, and Stefan Typel. Constraining the onset density of the hadron-quark phase transition with gravitational-wave observations. *Phys. Rev. D*, 102(12):123023, 2020.
- [27] Lukas R. Weih, Matthias Hanauske, and Luciano Rezzolla. Postmerger Gravitational-Wave Signatures of Phase Transitions in Binary Mergers. *Phys. Rev. Lett.*, 124(17):171103, 2020.
- [28] Andoni Torres-Rivas, Katerina Chatziioannou, Andreas Bauswein, and James Alexander Clark. Observing the post-merger signal of GW170817-like events with improved gravitational-wave detectors. *Phys. Rev. D*, 99(4):044014, 2019.
- [29] Marica Branchesi et al. Science with the Einstein Telescope: a comparison of different designs. *arXiv e-prints*, page arXiv:2303.15923, 3 2023.
- [30] Thibault Damour and Alessandro Nagar. Relativistic tidal properties of neutron stars. *Phys. Rev. D*, 80:084035, 2009.
- [31] Sergey Postnikov, Madappa Prakash, and James M. Lattimer. Tidal Love Numbers of Neutron and Self-Bound Quark Stars. *Phys. Rev. D*, 82:024016, 2010.
- [32] M. Sieniawska, W. Turczanski, M. Bejger, and J. L. Zdunik. Tidal deformability and other global parameters of compact stars with strong phase transitions. *Astron. Astrophys.*, 622:A174, 2019.
- [33] Sophia Han and Andrew W. Steiner. Tidal deformability with sharp phase transitions in (binary) neutron stars. *Phys. Rev. D*, 99(8):083014, 2019.

- [34] Katerina Chatziioannou and Sophia Han. Studying strong phase transitions in neutron stars with gravitational waves. *Phys. Rev. D*, 101(4):044019, 2020.
- [35] Hsin-Yu Chen, Paul M. Chesler, and Abraham Loeb. Searching for exotic cores with binary neutron star inspirals. *Astrophys. J. Lett.*, 893(1):L4, 2020.
- [36] J. F. Coupechoux, R. Chierici, H. Hansen, J. Margueron, R. Somasundaram, and V. Sordini. Impact of O4 future detection on the determination of the dense matter equations of state. *arXiv e-prints*, page arXiv:2302.04147, February 2023.
- [37] Philippe Landry, Reed Essick, and Katerina Chatziioannou. Nonparametric constraints on neutron star matter with existing and upcoming gravitational wave and pulsar observations. *Phys. Rev. D*, 101(12):123007, 2020.
- [38] Reed Essick, Ingo Tews, Philippe Landry, Sanjay Reddy, and Daniel E. Holz. Direct Astrophysical Tests of Chiral Effective Field Theory at Supranuclear Densities. *Phys. Rev. C*, 102(5):055803, 2020.
- [39] Peter T. H. Pang, Tim Dietrich, Ingo Tews, and Chris Van Den Broeck. Parameter estimation for strong phase transitions in supranuclear matter using gravitational-wave astronomy. *Phys. Rev. Res.*, 2(3):033514, 2020.
- [40] Jérôme Margueron, Rudiney Hoffmann Casali, and Francesca Gulminelli. Equation of state for dense nucleonic matter from metamodeling. i. foundational aspects. *Phys. Rev. C*, 97:025805, Feb 2018.
- [41] Nuclear matter with an equal number of protons and neutrons, i.e. $\delta = 0$.
- [42] J. L. Zdunik and P. Haensel. Maximum mass of neutron stars and strange neutron-star cores. *A&A*, 551:A61, March 2013.
- [43] Mark G. Alford and Armen Sedrakian. Compact stars with sequential QCD phase transitions. *Phys. Rev. Lett.*, 119(16):161104, 2017.
- [44] Nai-Bo Zhang and Bao-An Li. Properties of First-Order Hadron-Quark Phase Transition from Directly Inverting Neutron Star Observables. *arXiv e-prints*, page arXiv:2304.07381, April 2023.
- [45] Thomas Carreau, Francesca Gulminelli, and Jérôme Margueron. Bayesian analysis of the crust-core transition with a compressible liquid-drop model. *Eur. Phys. J. A*, 55(10):188, 2019.
- [46] D. G. Ravenhall, C. J. Pethick, and J. M. Lattimer. NUCLEAR INTERFACE ENERGY AT FINITE TEMPERATURES. *Nucl. Phys. A*, 407:571–591, 1983.
- [47] Toshiki Maruyama, Toshitaka Tatsumi, Dmitri . N. Voskresensky, Tomonori Tanigawa, and Satoshi Chiba. Nuclear pasta structures and the charge screening effect. *Phys. Rev. C*, 72:015802, 2005.
- [48] W. G. Newton, M. Gearheart, and Bao-An Li. A survey of the parameter space of the compressible liquid drop model as applied to the neutron star inner crust. *Astrophys. J. Suppl.*, 204:9, 2013.
- [49] Meng Wang, G. Audi, F. G. Kondev, W.J. Huang, S. Naimi, and Xing Xu. The AME2016 atomic mass evaluation (II). tables, graphs and references. *Chinese Physics C*, 41(3):030003, mar 2017.
- [50] H. Dinh Thi, T. Carreau, A. F. Fantina, and F. Gulminelli. Uncertainties in the pasta-phase properties of catalysed neutron stars. *Astron. Astrophys.*, 654:A114, 2021.
- [51] H. Dinh Thi, A. F. Fantina, and F. Gulminelli. The effect of the energy functional on the pasta-phase properties of catalysed neutron stars. *Eur. Phys. J. A*, 57(10):296, 2021.
- [52] S. Borhanian. GWBENCH: a novel Fisher information package for gravitational-wave benchmarking. *Classical and Quantum Gravity*, 38(17):175014, August 2021.
- [53] Curt Cutler and Eanna E. Flanagan. Gravitational waves from merging compact binaries: How accurately can one extract the binary’s parameters from the inspiral wave form? *Phys. Rev. D*, 49:2658–2697, 1994.
- [54] Eric Poisson and Clifford M. Will. Gravitational waves from inspiraling compact binaries: Parameter estimation using second-post-Newtonian waveforms. *Phys. Rev. D*, 52(2):848–855, July 1995.
- [55] Michele Vallisneri. Use and abuse of the Fisher information matrix in the assessment of gravitational-wave parameter-estimation prospects. *Phys. Rev. D*, 77(4):042001, February 2008.
- [56] Leslie Wade, Jolien D. E. Creighton, Evan Ochsner, Benjamin D. Lackey, Benjamin F. Farr, Tyson B. Littenberg, and Vivien Raymond. Systematic and statistical errors in a Bayesian approach to the estimation of the neutron-star equation of state using advanced gravitational wave detectors. *Phys. Rev. D*, 89(10):103012, May 2014.
- [57] Tanja Hinderer. Tidal Love Numbers of Neutron Stars. *Astrophys. J.*, 677(2):1216–1220, April 2008.
- [58] Tanja Hinderer. Erratum: “Tidal Love Numbers of Neutron Stars”. *Astrophys. J.*, 697(1):964, May 2009.
- [59] Jonas P. Pereira, Michał Bejger, Nils Andersson, and Fabian Gittins. Tidal Deformations of Hybrid Stars with Sharp Phase Transitions and Elastic Crusts. *Astrophys. J.*, 895(1):28, May 2020.
- [60] Katerina Chatziioannou, Carl-Johan Haster, and Aaron Zimmerman. Measuring the neutron star tidal deformability with equation-of-state-independent relations and gravitational waves. *Phys. Rev. D*, 97(10):104036, May 2018.
- [61] Hoa Dinh Thi, Chiranjib Mondal, and Francesca Gulminelli. The nuclear matter density functional under the nucleonic hypothesis. *Universe*, 7(10):373, 2021.
- [62] C. Mondal and F. Gulminelli. Nucleonic metamodeling in light of multimessenger, prex-ii, and crex data. *Phys. Rev. C*, 107:015801, Jan 2023.
- [63] Alekski Kurkela, Paul Romatschke, and Alekski Vuorinen. Cold Quark Matter. *Phys. Rev. D*, 81:105021, 2010.
- [64] Shu-Sheng Xu, Yan Yan, Zhu-Fang Cui, and Hong-Shi Zong. 2+1 flavors QCD equation of state at zero temperature within Dyson–Schwinger equations. *Int. J. Mod. Phys. A*, 30(36):1550217, 2015.
- [65] H. Chen, J. B. Wei, M. Baldo, G. F. Burgio, and H. J. Schulze. Hybrid neutron stars with the Dyson-Schwinger quark model and various quark-gluon vertices. *Phys. Rev. D*, 91(10):105002, 2015.
- [66] Andreas Zacchi, Matthias Hanauske, and Jürgen Schaffner-Bielich. Stable hybrid stars within a SU(3) Quark-Meson-Model. *Phys. Rev. D*, 93(6):065011, 2016.
- [67] D. E. Alvarez-Castillo, D. B. Blaschke, A. G. Grunfeld, and V. P. Pagura. Third family of compact stars within a nonlocal chiral quark model equation of state. *Phys. Rev. D*, 99:063010, Mar 2019.
- [68] Konstantin Otto, Micaela Oertel, and Bernd-Jochen Schaefer. Hybrid and quark star matter based on a nonperturbative equation of state. *Phys. Rev. D*, 101(10):103021, 2020.

- [69] Niko Jokela, Matti Järvinen, Govert Nijs, and Jere Remes. Unified weak and strong coupling framework for nuclear matter and neutron stars. *Phys. Rev. D*, 103(8):086004, 2021.
- [70] Mahboubeh Shahrbafl, Sofija Antić, A. Ayriyan, David Blaschke, and Ana Gabriela Grunfeld. Constraining free parameters of a color superconducting nonlocal Nambu–Jona-Lasinio model using Bayesian analysis of neutron stars mass and radius measurements. *Phys. Rev. D*, 107(5):054011, 2023.
- [71] C. Drischler, K. Hebeler, and A. Schwenk. Asymmetric nuclear matter based on chiral two- and three-nucleon interactions. *Phys. Rev. C*, 93:054314, May 2016.
- [72] B. P. Abbott et al. Properties of the binary neutron star merger GW170817. *Phys. Rev. X*, 9(1):011001, 2019.
- [73] Feryal Özel and Paulo Freire. Masses, Radii, and the Equation of State of Neutron Stars. *Ann. Rev. Astron. Astrophys.*, 54:401–440, 2016.
- [74] Robert E. Kass and Adrian E. Raftery. Bayes factors. *Journal of the American Statistical Association*, 90(430):773–795, 1995.